A Finite Deformation Anisotropic Plasticity Model for Fiber Reinforced Composites

H. D. ESPINOSA, H. C. LU, S. K. DWIVEDI AND P. D. ZAVATTIERI

ABSTRACT

A total lagrangian explicit formulation is presented to model the large deformation response of fiber reinforced composite material to impact and penetration. The inelastic response of each ply is described by an anisotropic rate dependent plasticity model. The parameters of the anisotropic constitutive model are determined experimentally using the off-axis and the Arcan shear tests. The interface between plies is treated separately through a contact/interface algorithm which takes into account delamination, opening and subsquent closing of the interface and large sliding between plies. The response parameters of the interface elements are modelled in terms of the actual materials properties. Hence, attempt has been made to model the pre- and post-failure response of fiber reinforced composite targets based on exprimentally observed failure mechanisms. The formulation is thought to simulate the penetration of GRP composite plates at impact velocities in the range of 180-200 m/s, Espinosa et al. 1996.

INTRODUCTION

Fibre reinforced composite materials have gained prominence as advanced materials owing to their high stiffness/density and strength/ density ratio. Specially, the glass fibre reinforced plastic (GRP) has become the potential material for designing weight efficient armor systems and combat vehicles. It becomes compulsary to evaluate their structural integrity under dynamic conditions at high strain rates before making full utilization in such applications.

The overall energy absorbing capability of fibre reinforced materials depend upon their consituents which include fibers, matrix, fibre-matrix interface and interface between plies. There have been a spate of studies over the last decade to gain insight into the failure mechanisms induced by impact damage in fiber- reinforced composite materials. Different failure modes including delamination, interlaminar matrix cracking, fiber/matrix debonding, fiber breakage and fiber pull-out have been observed. At low velocity impact, matrix fracture and interply delamination have been found to govern the damage of composites. While, extensive fiber fracture and microbuckling have been observed at high velocity

[0]Horacio Dante Espinosa, Associate Professor; Hung Chen Lu, Reseaech Assistant; Sunil Kumar Dwivedi, Post-Doctoral Researcher; Pablo D. Zavattieri, Research Assistant; School of Aeronautics and Astronautics, Purdue University, West Lafayette, IN 47907-1282

impact. In the latter case, the magnitude and extent of damage is a function of the penetrator shape and mass, striking velocity, plate thickness, and composite constituents' properties.

For instance, higher fiber strength provide better impact resistance to composites (Broutman and Rotem, 1975). According to Beaumont, 1979, the post-debond fiber sliding is the primary energy absorbing mechanism in glass fiber-reinforced composites, whereas fiber pull-out is responsible for much of the toughness in a carbon fiber composite. On the other hand, the tensile strength of the matrix material has a significant effect on impact behavior (Williams and Rhodes, 1982, Hunston, 1984, Elber, 1985). The matrix properties govern the damage threshold and determine the extent of impact damage while the fibre properties govern the resistance to penetration. The toughness of matrix is fully transferred to the toughness of composite for brittle polymers, while only partial transfer takes place for tougher polymers resins. Similarly, the interface between matrix and ply and those between plies affect the impact resistance of composites. The transverse fracture energy of a composite directly depends on the matrix-ply bond strength (Dorey, 1980, Ying, 1983). Measures to increase the interply bond strength have been suggested to enhance the impact resistance of composites (Sun and Rechak, 1988, Pelstring and Madan, 1989).

Additionally, numerical techniques have been used to study the impact resistance of fiber- reinforced composites. Lee and Sun, 1993a and b, studied the damage mechanisms of AS4/PEEK composites under quasi-static penetration experiments and established the load-deflection relation. This was used in a dynamic analyses to determine the ballistic limit of graphite/epoxy laminates. A comprehensive review of experimental as well as numerical work can be found in Abrate 1991, 1994 and Cantwell and Norton, 1991.

The response of fiber reinforced composite materials is a complex function of many factor, e.g., strength of matrix vis-a-vis fiber, fiber orientation, failure mechanism such as delamination, fiber breakage, fiber pull out, and the material post-failure response. One type of composite material may behave quite differently from another under the same load. Furthermore, recent experimental findings have been found to be contradictory to some of past experimental results, which in part may be due to the advancement of the measurement techniques. While there have been very few attempts to simulate the penetration of composite targets through modelling of non-linear phenomena, e.g., constitutive behavior, failure, delamination, contact/friction, etc. These new findings prompted the need for experimental as well as numerical investigations dealing with damage resistance and damage tolerance of fiber composites.

The approach is to understand the response of composite materials to impact loading through experiments and translate the findings to numerical simulations through proper modelling of inelasticity and pre- and post-failure constitutive behavior for full scale design and analyses. With this in view, Espinosa et al., 1996, devised a new technique for recording projectile tail velocity histories using a normal velocity interferometer (NVI) and target back surface velocity with multi-point interferometry. The technique has been used to study the dynamic failure mechanisms of woven fiber-reinforced plastic laminates (GRP) made of S-2 glass fibres embedded in a polyester resin matrix with approximately 60% fiber by volume. The penetration experiments have been carried out with the conical shaped penetrator having rounded head in the velocity range of 180-200 m/s. Three

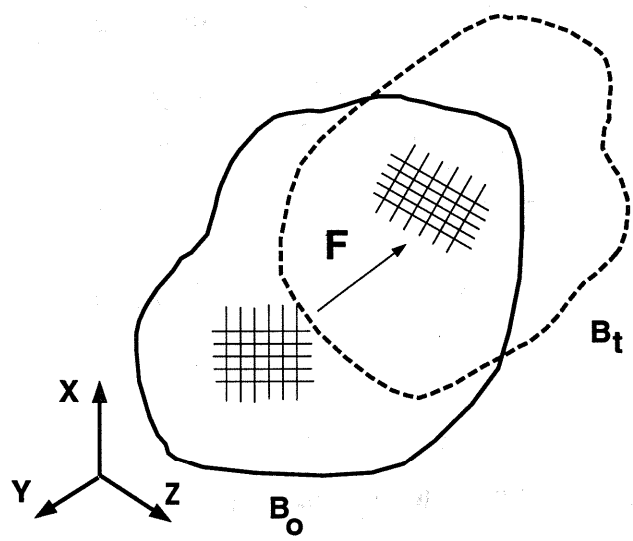

Figure 1: **Total Lagrangian Continuum Model**

distinctive zones of failure have been observed which includes extensive delaminations and fiber shearing, tensile fiber failure and large fiber deflection and lastly fiber microfracture and buckling.

In parallel, Espinosa and co-workers developed a multiple-plane microcracking model to describe the inelastic response of ceramics and a versatile contact algorithm with cohesive interface to deal with the complex situations involving debonding, large sliding and subsquent closing and opening of interfaces, Espinosa et al., 1996, 1997. The contact-interface model has been applied to simulate the delamination/contact of GRP plates as studied experimentally. A finite deformation anisotropic plasticity model was formulated and experiments carried out to determine the anisotropic model parameters of GRP. The mathematical formulation and experimental results are given in the following sections.

FORMULATION

It is evident from the above that the deformation of composite materials during impact and penetration is predominantly large involving large rotations and failure through various mechanisms. A total lagrangian continuum model as shown in Figure 1 has been adopted in the present formulation.

The large deformation and rotations of material are accounted through the energy conjugate second Piola Kirchoff's stress and Green Lagrnage's strain tensors in the initial undeformed configuration B_0. The constitutive behavior of the material is determined experimentally and included in the model. Additionally, a contact/ interface model is developed to deal with the phenomena of delamination during the deformation. As shown in Figure 2, the interface may be intact at time t_0. It may break and the plies separate at time t_1. As a result, one may have the situation of local delamination and/or a progressing front of delamination. The delaminated plies may come in contact as shown at time t_2

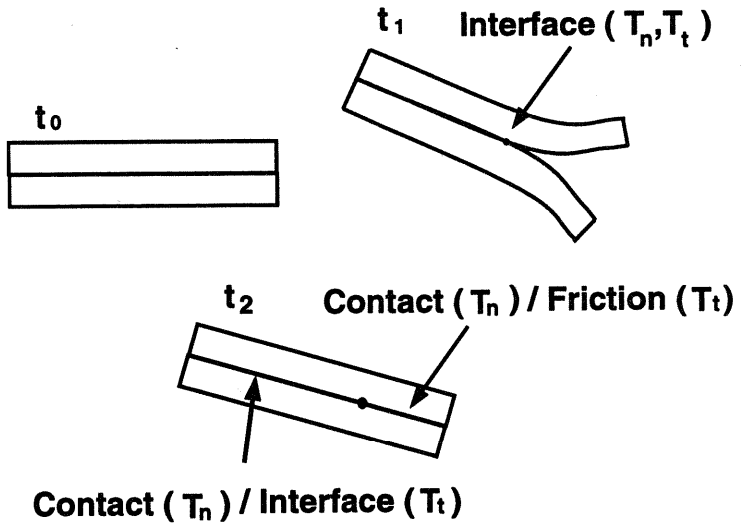

Figure 2: **Interface/Contact Model with Finite Kinematics**

and slide under compressive tractions involving frictional effects. The large deformation contact/interface model takes into account all these phenomena to predict the response of composite materials closer to reality.

FIELD EQUATIONS AND FINITE DEFORMATION ANISOTROPIC PLASTICITY MODEL

The rate form of virtual work equation in total lagrangian formulation, describing the motion from time step n to $n+1$, is given as,

$$\int_{B_0} \Delta\epsilon_{ij} L_{ijkl} \delta\epsilon_{rs} dB_0 + \int_{B_0} S_{ij_{(n)}} \delta\eta_{ij} dB_0 - \int_{B_o} \rho_o(\mathbf{b_i} - \mathbf{a_i}) \delta u_i dB_o - \int_{S_{o\sigma}} \mathbf{t} \delta u_i dS_o = 0 \quad (1)$$

where, S_{ij} is the second Piola Kirchoff's stress components, ϵ_{ij} and η_{ij} are the linear and non-linear components of the Green lagrange strain rate $\dot{E}_{ij}$, b_0, a and t are the body force vector, acceleration vector and boundary traction vector and superscript n indicates the value at time step n. In the absence of the body force and boundary traction, the above equation can be written at time step n for the explicit integration as,

$$M\ddot{U} = -F_{int} \quad (2)$$

where M is the global mass matrix, $\ddot{U}$ is the global acceleration vector and F_{int} is the internal force vector. The impactor as well as all the layers of composite target are discretized spatially into six node quadratic triangular elements. The mass of triangle is lumped at their nodes to get the global lumped mass matrix. Details on the numerical integration of the above equations can be found in Espinosa et al., 1996, 1997.

Assuming linear variation from time step n to $n+1$, the Green lagrange strain rate at new time step $n+1$ is given as,

$$\dot{E}_{ij} = \frac{1}{2\Delta t}[(F_{ki}F_{jk})_{n+1} - (F_{ki}F_{jk})_n] \tag{3}$$

where F_{ij} is the deformation gradient and Δt is the incremental time step. All quantities in the above equation are defined in the global co-ordinates. The second Piola Kirchoff's stress rate tensor is given by the constitutive law,

$$\dot{S}_{ij} = L_{ijkl}\dot{E}^e_{kl} \tag{4}$$

where L_{ijkl} is the elastic anisotropic material stiffness constitutive tensor in the global co-ordinates and $\dot{E}^e_{ij}$ is the elastic component of the Green lagrange strain rate tensor. In the case of anisotropic materials, the elastic constitutive matrix (L_l) is defined in the local co-ordinate system of the ply (Cook, R.D.,1974). It is tranformed to $L = T^T L_l T$ to obtain the constitutive matrix in the global co-ordinates following standard transformation proceedures.

The elastic components of the strain rate tensor are obtained by an additive decomposition of the total strain rate, namely,

$$\dot{E}^e_{ij} = \dot{E}_{ij} - \dot{E}^p_{ij} \tag{5}$$

In the above equation, $\dot{E}^p_{ij}$ is the plastic strain rate which is given based on the associative flow rule as,

$$\dot{E}^p_{ij} = \dot{\lambda}\frac{\partial f}{\partial S_{ij}} \tag{6}$$

Here, f is the flow potential and $\dot{\lambda}$ is the plastic rate proportionality factor. The inelastic behavior of the composite is modeled based on the small deformation yield function, quadratic in stresses, as proposed by Sun and Chen, 1989, i.e., Hill's type potential.

$$\begin{aligned} 2f(S_{ij}) \;=\; & a_{11}S^2_{11} + a_{22}S^2_{22} + a_{33}S^2_{33} \\ & +2a_{12}S_{11}S_{22} + 2a_{13}S_{11}S_{33} + 2a_{23}S_{33}S_{22} \\ & +2a_{44}S^2_{23} + 2a_{55}S^2_{13} + 2a_{66}S^2_{12} \end{aligned} \tag{7}$$

Experimental evidences show that the fiber composites behave linearly up to failure if the load is applied in the fiber direction. Hence, for orthogonal fibers oriented along direction 1 and 2, it is assumed that $E^p_{11} = E^p_{22} = 0$. The above flow potential then reduces to,

$$f(S_{ij}) = \frac{1}{2}S^2_{33} + a_{44}S^2_{23} + a_{55}S^2_{13} + a_{66}S^2_{12} \tag{8}$$

For equal fiber volume fractions in the principal 1 and 2 directions, the additional constraint of $a_{44} = a_{55}$ is obtained which further reduces the yield function to,

$$f(S_{ij}) = \frac{1}{2}S^2_{33} + a_{44}(S^2_{23} + S^2_{13}) + a_{66}S^2_{12} \tag{9}$$

Defining an effective stress as,

$$\bar{S} = \sqrt{3f} \tag{10}$$

and using equations (7) and (10) and the rate of plastic work given by,

$$\dot{W}^p = S_{ij}\dot{E}^p_{ij} = \bar{S}\dot{\bar{E}}^p. \tag{11}$$

The proportionality factor of equation (6) is obtained as

$$\dot{\lambda} = \frac{3\dot{\bar{E}}^p}{2\bar{S}} \tag{12}$$

where $\dot{\bar{E}}^p$ is the effective plastic strain rate. The effect of strain rate and temperature can be modeled by defining the material strength in terms of an effective stress which includes temperature and rate terms, namely,

$$\dot{\bar{E}}^p = \dot{\bar{E}}^p_0[\frac{\bar{S}}{g(\bar{E}^p, T)}]^m \quad \text{if} \quad \bar{S} > g(\bar{E}^p, T) \tag{13}$$

$$g(\bar{E}^p, T) = \bar{S}_y[1 - (\frac{T - T_0}{T_m - T_0})^\alpha] \tag{14}$$

$\bar{S}_y$ in the above equation is the flow stress and is defined by an experimentally found power law, viz.,

$$\bar{S}_y = (\frac{\bar{E}^p}{A})^{1/n} \tag{15}$$

A summary of the constitutive equations is given in Table 1.

EXPERIMENTAL DETERMINATION OF THE ANISOTROPIC MODEL PARAMETERS

The anisotropic yield function given in equation (9) involves two coefficients which need to be determined experimentally. Following Sun and Chen, 1989, the coefficient a_{66} is determined from off-axis tensile tests to obtain a master effective stress-effective plastic strain curve.

As shown in Figure 3, let X axis be the uniaxial loading direction which makes an angle θ with respect to the fiber direction X_1. The stress referring to the material principle axes are

$$\begin{aligned} S_{11} &= cos^2\theta S_x \\ S_{22} &= sin^2\theta S_x \\ S_{12} &= -sin\theta cos\theta S_x \end{aligned} \tag{16}$$

where S_x is the applied axial stress. For the case of 2-D plane stress parallel to the X_1-X_2 plane, the plastic potential function can be reduced to,

$$f(S_{ij}) = a_{66}S^2_{12} \tag{17}$$

Table 1: **Summary of constitutive equations**

$$\dot{S}_{n+1} = L\dot{E}^e_{n+1}$$

$$\dot{E}_{n+1} = \dot{E}^e_{n+1} + \dot{E}^p_{n+1}$$

$$\dot{E}^p_{n+1} = \dot{\lambda}\frac{\partial f}{\partial S_{n+1}} = \frac{3\dot{\bar{E}}^p}{2\bar{S}}\frac{\partial f}{\partial S_{n+1}} = \dot{\bar{E}}^p_{n+1}N_{n+1}$$

$$N_{n+1} = \frac{\frac{3}{2}\frac{\partial f}{\partial S_{n+1}}}{\bar{S}_{n+1}} = \frac{3}{2\bar{S}}\begin{bmatrix} 0 & 2a_{66}S_{12} & 2a_{55}S_{13} \\ 2a_{66}S_{12} & 0 & 2a_{44}S_{23} \\ 2a_{55}S_{13} & 2a_{44}S_{23} & S_{33} \end{bmatrix}_{n+1}$$

$$\bar{S}_{n+1} = \sqrt{3f_{n+1}(S_{ij})_{n+1}}$$

$$g(\bar{E}^p_{n+1}, T) = \bar{S}_{y,n+1}[1 - (\frac{T-T_0}{T_m-T_0})^\alpha]$$

$$\bar{S}_{y,n+1} = (\frac{\bar{E}^p_{n+1}}{A})^{\frac{1}{n}}$$

$$\dot{\bar{E}}^p_{n+1} = \dot{\bar{E}}^p_0[\frac{\bar{S}_{n+1}}{g(\bar{E}^p_{n+1}, T)}]^m$$

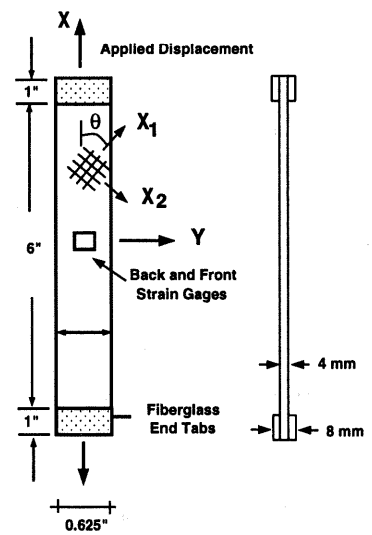

Figure 3: **Off-axis tensile test specimen**

Substituting the above equation into the effective stress equation, the effective stress can be derived in term of the stress S_x and the fiber direction θ, namely,

$$\bar{S} = \sqrt{3a_{66}cos^2\theta sin^2\theta}S_x = h(\theta)S_x \tag{18}$$

where, $h(\theta) = \sqrt{3a_{66}cos^2\theta sin^2\theta}$ is a function of the fiber orientation θ. The relationship between the incremental plastic strain and stress in term of the current state of stress reduces to,

$$\dot{\bar{E}}^p = \frac{2}{3}\bar{S}\dot{\lambda} = \frac{2}{3}h(\theta)S_x\dot{\lambda}. \tag{19}$$

The inelastic strain components are derived by substituting the yield function into the associated flow equation and are given by,

$$\begin{bmatrix} \dot{E}^p_{11} \\ \dot{E}^p_{22} \\ 2\dot{E}^p_{12} \end{bmatrix} = \begin{bmatrix} 0 \\ 0 \\ 2a_{66}S_{12}\dot{\lambda} \end{bmatrix} \tag{20}$$

Using coordinate transformations, equation for the strain in the X direction can be derived as,

$$\begin{aligned} \dot{E}^p_x &= cos^2\theta\dot{E}^p_{11} + sin^2\theta\dot{E}^p_{22} - 2cos\theta sin\theta\dot{E}^p_{12} \\ &= 2a_{66}cos\theta sin\theta S_x\dot{\lambda} = \frac{2}{3}h^2(\theta)S_x\dot{\lambda} \end{aligned} \tag{21}$$

Comparing the above equation with the equation of the effective strain, the relationship between the effective strain and the plastic strain component in X direction is obtained as,

$$\dot{\bar{E}}^p = \frac{\dot{E}^p_x}{h(\theta)} \tag{22}$$

Integrating both sides, the relation between the plastic strain in the X direction and effective plastic strain can be obtained,

$$\bar{E}^p = \frac{E^p_x}{h(\theta)} \tag{23}$$

The above equations provide an useful relation to characterize the ratio between effective stress and effective plastic strain.

$$\frac{\bar{S}}{\bar{E}^p} = h^2(\theta)\frac{S_x}{E^p_x} \tag{24}$$

Hence, determining the variation of S_x v.s. E^p_x experimentally , the variation of $\bar{S}$ v.s. $\bar{E}^p$ can be obtained from the above relation.

The effective stress-effective plastic strain relation needs to be unique in monotonic loading for a given material and strain rate. The parameter a_{66} is chosen so that the

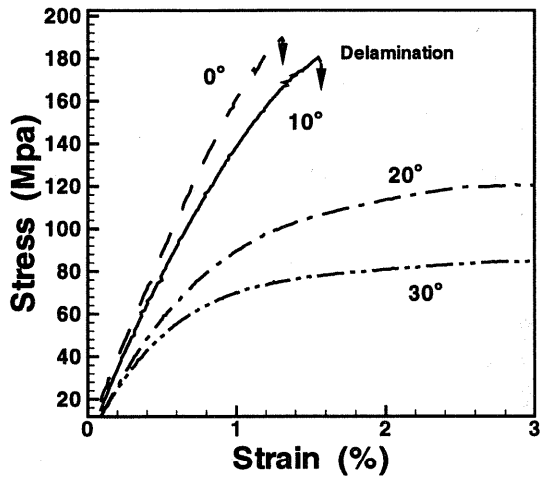

Figure 4: **Experimental stress-strain curves from off-axis tension tests**

resulting effective stress- effective plastic strain is independent of the off-axis angle θ. Experimental results have indicated that thermoplastic composites do not have a well-defined yield point so that the master effective stress-effective plastic strain curve can be fitted with a power law

$$\bar{E}^p = A(\bar{S})^n \tag{25}$$

where the power law coefficient **A** and **n** can be obtained by the curve fitting.

Experiments have been carried out at four different values of θ as 0, 10, 20 and 30. The S_x v.s. E_x curve obtained are shown in the Figure 4. Figure 5 shows the variation of $\bar{S}$ v.s. $\bar{E}^p$. Values of **A** and **n** have been obtained by fitting two curves as shown in the figure with their values.

The other coefficient, a_{44}, is related to the behavior of the composite when subjected to out-of-plane shearing. Its value can be identified from a pure shear loading obtained with an Arcan loading fixture, Arcan et al., 1978. The potential function for a pure shear test in the **1-3** direction can be simplified as,

$$f(S_{ij}) = a_{44}S_{13}^2 \tag{26}$$

since the rest of the stress components are equal to zero. By using the definition of effective stress, the relation between the effective stress and applied stress can be found as,

$$\bar{S} = \sqrt{3a_{44}}S_{xz} = \sqrt{3a_{44}}S_{13} \tag{27}$$

Applying the associated flow rule, the strain component in the **1-3** direction can be calculated in terms of the applied stress S_{xz},

$$\dot{E}_{13}^p = 2a_{44}S_{13}\dot{\lambda} \tag{28}$$

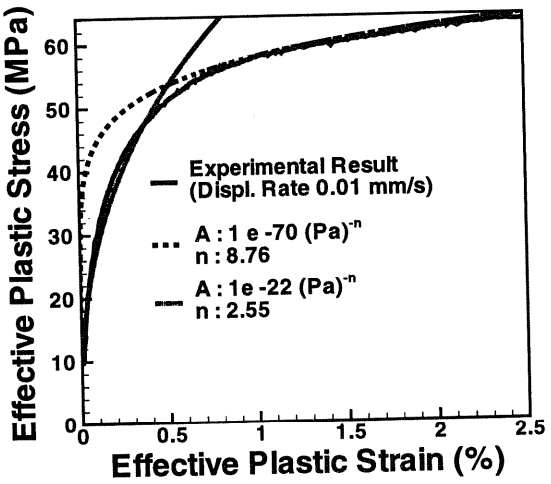

Figure 5: **Effective stress vs. effective plastic strain**

with

$$\dot{\lambda} = \frac{\dot{E}^p_{13}}{2a_{44}S_{13}} \tag{29}$$

The effective plastic strain rate can be related to the strain component S_{13} by the following expression,

$$\dot{\bar{E}}^p = \frac{2}{3}\bar{S}\dot{\lambda} = \frac{\dot{E}_{13}}{3a_{44}} \tag{30}$$

The relationship between the effective plastic strain and the experimentally measured strain can be found to be,

$$\bar{E}^p = \frac{E_{13}}{3a_{44}} \tag{31}$$

The stress and strain relation between the effective values and experimental values can thus be built as

$$\frac{\bar{S}}{\bar{E}^p} = \frac{3a_{44}S_{13}}{E^p_{13}} \tag{32}$$

Based on the above equations, the coefficient a_{44} can be obtained by matching the power law curve dentified through off-axis tests. Figure 6 shows the Arcan fixture used in our experiments.

CONTACT / INTERFACE MODEL

The above model is integrated with a dynamic contact/interface model. A versatile multi-body contact model for explicit dynamic analysis have been developed. The penetration of nodes of one body, i.e., slave nodes into the surface of other body, i.e., master

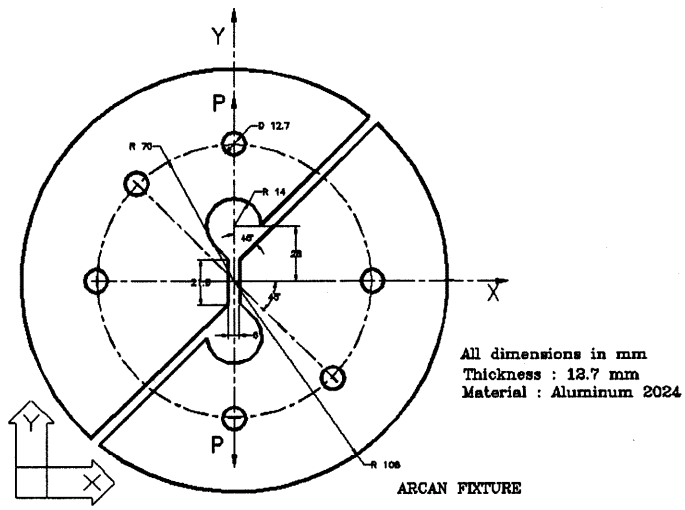

Figure 6: **Arcan's experiment for pure shear loading, Arcan et al., 1978.**

surface is checked. If found penetrating, then the force required to impose the impenetrability condition is applied to the slave nodes. The equal and opposite force is applied to master surface and properly distributed to its nodes to maintain the conservation of force. Tangential forces arising from Coulomb's friction, in which a friction coefficient is taken as the function of the relative sliding velocity, are also applied on the surface. A detailed description of the contact model can be found in Espinosa et al., 1996, 1997.

The contact model is integrated with an interface elements to simulate the delaminations and subsquent large sliding, opening and closing of the interface. The model is based on the interface model proposed by Tvergaard, 1990 for quasi-static calculations. It assumes that the interface carried forces that oppose separation and shear between two surfaces until debonding. The magnitude of these forces are function of the relative separation and shear displacement between the two surfaces. The normal and tangential tractions are given as,

$$T_n = \frac{u_n}{\delta_n} F(\lambda_c), \quad T_t = \alpha \frac{u_t}{\delta_t} F(\lambda_c) \tag{33}$$

$$F(\lambda_c) = \frac{27}{4} T_{max}(1 - 2\lambda_c + {\lambda_c}^2), \quad \text{for} \quad 0 \leq \lambda_c \leq 1 \tag{34}$$

where, λ_c is a non-dimensional parameter given as,

$$\lambda_c = \sqrt{\left(\frac{u_n}{\delta_n}\right)^2 + \left(\frac{u_t}{\delta_t}\right)^2} \tag{35}$$

In the above equation, u_n and u_t are the normal and tangential displacement jumps at the interface. δ_n and δ_t are critical values at which delamination takes place. T_{max} and δ_n and δ_t can be easily determined from energy arguments based on the mode I critical strain energy release rate of the interface. It is evident that the value of λ_c varies from **0** to **1**

Table 2: **Contact and Interface calculations based on interface traction**

LOAD	STATE	T_n	T_t
TENSION-SHEAR	$\lambda < 1$	Interface	Interface
	$\lambda \geq 1$	Contact	Open
COMPRESSION-SHEAR	$\lambda < 1$	Contact	Interface
	$\lambda \geq 1$	Contact	Friction

with $\lambda_c = 1$ defining interface failure (delamination). Four node quadrilateral elements are embedded as the interface elements between plies. The normal and tangential forces are computed depending upon the state of stress at the interface as shown in Figure 2 and Table 2.

As long as the value of λ_c remains less than unity, the interface normal traction is computed from contact model in the case of compression-shear and from interface model in the case of tension-shear. The shear traction is computed from the interface model. For values of λ_c larger than unity, delamination case, only the contact model is used to compute the interface tractions in both the states. The dependance of the interface model on the materials properties and swithching from interface to contact and vise versa make the approach realistic to simulate the delamination and subsqunet large sliding at the interface between plies. Rate effects in the delamination process can be easily incorporated in terms of the λ_c parameters as given by,

$$T_{max} = T^o_{max}(1 + \beta \ln[\frac{\dot{\lambda}_c}{\dot{\lambda}_{c,o}}]) \quad \text{with} \quad T^o_{max} = \frac{48 G_c}{27 \delta_n} \tag{36}$$

ACKNOWLEDGMENTS

This research was supported by the National Science Foundation through Grants Nos. MSS-9309006 and MSS 9311289, and by the Army Office of Scientific Research under Grant DAAH 04-95-1-0168 and Purdue-MURI'96.

REFERENCES

Abrate, S., 1991, "Impact on laminated composite materials" *Applied Mechanics Review, American Society of Mechanical Engineers* 44(4):155-189.

Abrate, S., 1994, "Impact on laminated composites: Recent Advances" *Applied Mechanics Review, American Society of Mechanical Engineers* 47(11):517-544.

Beaumont, P.W.R., 1979, "Fracture Mechanisms in Fibrous Composites," Fracture Mechanics, Current Status, Fracture Prospects edited by R. A. Smith (Pergamon Press), 211-233.

Broutman, LJ., and Rotem, A., 1975, "Impact Strength and Toughness of Fiber Composite Materials," Foreign Object Impact Damage to Composites, American Society for Testing and Materials, ASTM STP 568:114-133.

Cantwell, W.J., and Norton, J.. 1991. "The Impact Resistance of Composite Materials - A Review" *Composites,* 22(5):347-362.

Cook, R. D., 1974, "Concpets and Applications of Finite Element Analysis", John Willey and Sons Inc., New York.

Dorey, G., 1980, "Relationship between Impact Resistant and Fracture Toughness in Advanced Composite Materials," Effect of Service Environment on Composite Materials, *AGARD CP 28*

Elber, W., 1985, "Failure mechanics in Low Velocity Impact on Thin Composite Plates," *NASA Techical Paper 2152.*

Espinosa, H. D., Lu, H-C. and Xu, Y., 1996, "A novel technique for penetration velocity measurement and damage identification in ballistic penetration experiments." *to appear in J. Composite Materials.*

Espinosa, H.D., Emore, G.L., and Zavattieri, P.D., 1996, "Computational Modeling of Geometric and Material Nonlinearities with an Application to Impact Damage in Brittle Materials," *in Advances in Failure Mechanisms in Brittle Materials,* edited by R.J. Clifton and H.D. Espinosa, AMD-Vol. 219, MD-Vol 75, pp. 119-161.

Espinosa, H.D., Zavattieri, P.D. and Emore, G.L., 1997, "Adaptive FEM computation of geometric and material nonlinearities with application to brittle failure." *to appear in the Special Issue of Mechanics of Materials.*

Hunston, D.L., 1984, "Composite Interlaminar fracture ; Effect of matrix Fracture Energy," *Composites Tech Review 6*:176-180.

Lee, S-W. R., and Sun, C.T., 1993a, "A Quasi-Static Penetration Model for Composite Laminates", *J. of Composite Materials*, 27:251-271.

Lee, S-W. R., and Sun, C.T., 1993b, "Dynamic Penetration of Graphite/Epoxy Laminates Impacted by a Blunt-Ended Projectile," *Composites Science and Technology*, 49:369-380.

Williams, J.G. and Rhodes, M.D., 1982, "Effect of resin on Impact Damage Tolerance of Graphite/Epoxy Laminateds" Composite Materials: testing and Design (sixth Conference), American Society for Testing and Materials, ASTM STP 787, edited by Daniel, I.M., 450-480.

Ying, L., 1983, "Role of Fiber/Matrix Interphase in Carbon Fiber Epoxy Composite Impact Toughness," *SAMPE Quart.*, 14(3):26.